

Finding Archetypal Spaces for Data Using Neural Networks

David van Dijk ^{*12} Daniel Burkhardt ^{*1} Matthew Amodio ² Alex Tong ² Guy Wolf ³ Smita Krishnaswamy ¹²

Abstract

Archetypal analysis is a type of factor analysis where data is fit by a convex polytope whose corners are “archetypes” of the data, with the data represented as a convex combination of these archetypal points. While archetypal analysis has been used on biological data, it has not achieved widespread adoption because most data are not well fit by a convex polytope in either the ambient space or after standard data transformations. We propose a new approach to archetypal analysis. Instead of fitting a convex polytope directly on data or after a specific data transformation, we train a neural network (AAnet) to learn a transformation under which the data can best fit into a polytope. We validate this approach on synthetic data where we add nonlinearity. Here, AAnet is the only method that correctly identifies the archetypes. We also demonstrate AAnet on two biological datasets. In a T cell dataset measured with single cell RNA-sequencing, AAnet identifies several archetypal states corresponding to naive, memory, and cytotoxic T cells. In a dataset of gut microbiome profiles, AAnet recovers both previously described microbiome states and identifies novel extrema in the data. Finally, we show that AAnet has generative properties allowing us to uniformly sample from the data geometry even when the input data is not uniformly distributed.

1. Introduction

Archetypal analysis, first developed in Cutler & Breiman (1994), is a type of factor analysis where the factors are constrained to be extrema of data, which are considered as “archetypes” (ATs). The concept of archetypal analysis has

proven useful in describing data geometry, especially in biological systems such as evolutionary trade-off (Shoval et al., 2012; Kavanagh et al., 2013; Tendler et al., 2015), gene expression (Hart et al., 2015; Korem et al., 2015), phenotypic state space (Sheftel et al., 2013), and life history trait space (Szekely et al., 2015). However, traditional approaches to archetypal analysis compute archetypes by fitting a linear convex hull to the data (Mørup & Hansen, 2012; Chen et al., 2014; Cutler & Breiman, 1994). While the concept of a fitting a linear hull may at times be useful and yields insightful results, it is often inapplicable to nonlinearly shaped data, where collected measurements do not naturally fit in the shape of a convex polytope. Such datasets require nonlinear transformations to produce a representation that is amenable to fitting a convex hull. Indeed, some archetypal analysis methods (e.g., kernel PCHA by Mørup & Hansen, 2012) try to find archetypes in a precomputed embedded space provided by kernel methods, such as Laplacian eigenmaps (Belkin & Niyogi, 2002). Others apply the fitting in the representation provided by a hidden layer found in a ConvNet pre-trained for classification (Wynen et al., 2018). Here, the archetypal analysis is performed in a fixed space that is not optimized for representing archetypes and therefore there is no guarantee that this representation of the data is well-fit by a convex polytope. Indeed, we demonstrate that the latent spaces learned by neural networks are not well-fit by such models (see Section 4). These existing methods treat the transformation of the data as a pre-processing step, instead of learning the transformation and archetypes simultaneously.

Here, we introduce a new approach to archetypal analysis by aiming to find a *new feature space* where the data naturally forms a convex polytope. To compute such a space, we introduce an archetypal analysis neural network, or AAnet. The AAnet is based on an autoencoder with a novel constraint on the embedding layer that we term *archetypal regularization*. This regularization trains the neural network to search through the space of non-linear transformations to learn a new feature-space where the data fits in a convex hull. In this space, the data gives rise to emergent archetypal structure rather than forcing a specific transformation of the data into a convex hull in a fixed feature space.

We show that AAnet can correctly find archetypes in non-linear data where linear archetypal analysis methods fail

^{*}Equal contribution ¹Department of Genetics, Yale University, New Haven, Connecticut, USA ²Department of Computer Science, Yale University, New Haven, Connecticut, USA ³Department of Mathematics & Statistics, Université de Montréal, Montreal, QC, Canada. Correspondence to: David van Dijk <david.vandijk@yale.edu>, Smita Krishnaswamy <smita.krishnaswamy@yale.edu>.

and that AAnet is more scalable than linear methods. Further, we show that archetypes obtained by this method are interpretable, as shown on benchmark data, newly measured single-cell data of tumor infiltrating lymphocytes, and gut microbiome samples. Finally, we show that using AAnet we can sample uniformly from the geometry, giving AAnet the ability to infer data in sparse regions of the data manifold, unlike GANs or VAEs which simply replicate data density.

The main contributions of this paper are the following: 1. A new autoencoder-based framework, named AAnet, for finding a transformation of the data feature space such that the transformed data lies in a convex polytope whose corners are meaningful archetypal points of the data. 2. A novel regularization that enforces a regular convex polytope shape on the embedding layer 3. A method for selecting the appropriate number of archetypes for a dataset via an elbow-plot analysis. 4. Ability to generate data from the geometry rather than density via sampling of the embedding layer of AAnet 5. Demonstrations of performance, robustness, and accuracy on several synthetic and biological datasets

2. Previous work and Background

The first algorithm proposed for archetypal analysis was principal convex hull analysis (PCHA) in Cutler & Breiman (1994), which solves the following optimization problem:

$$\begin{aligned} \operatorname{argmin}_{c_1, \dots, c_k} \quad & \sum_{i=1}^n \|x_i - \sum_{j=1}^k \alpha_{ij} c_j\|^2 \\ \text{s.t.} \quad & c_j = \sum_{i=1}^j \beta_{ji} x_i, \quad j = 1, \dots, k \end{aligned} \quad (2.1)$$

$$\begin{aligned} \sum_{j=1}^k \alpha_{ij} &= 1, \quad i = 1, \dots, n \\ \sum_{i=1}^n \beta_{ji} &= 1, \quad i = 1, \dots, n \\ \alpha_{ij} &\geq 0, \beta_{ji} \geq 0, \quad i = 1, \dots, n, \quad j = 1, \dots, d \end{aligned}$$

Here, $X = \{x_1, \dots, x_n\} \in \mathbb{R}^N$ is the set of data points. The task of archetypal analysis is to find d archetypes c_1, \dots, c_k such that each data point is a convex combination of these archetypes. The archetypes are, in turn, also convex combinations of the data points with coefficients β_{ji} .

Mørup & Hansen (2012) propose to solve the PCHA optimization via projected gradient descent. Further improvement to the optimization procedures are formed in Chen et al. (2014), which uses an active set strategy. More recently, Javadi & Montanari (2017) tighten envelope constraints by adding a cost for the sum of the distances of the

data points from the convex envelope of the archetypes and another for the sum of the distances of archetypes from the convex envelope of the data points.

Mørup & Hansen (2012) is one of the two works that perform archetypal analysis in a transformed feature space: the Eigenspace of a radial basis Kernel formed by pairwise relationships between data points. In Wynen et al. (2018), the authors perform archetypal analysis on the representation found in a hidden layer of an image classification neural network in order to define image styles. We note that these works still perform archetypal analysis in fixed space that is not optimal for archetypal analysis. By contrast, in our method we aim to *find* a nonlinear transformation of the data that makes the data optimally described by a convex polytope, and propose to use a novel neural network regularization for this task.

3. Archetypal Analysis Network (AAnet)

First, we describe our new generalized problem formulation for finding a transformed data space for archetypal analysis, and then we describe our AAnet autoencoder framework.

3.1. Problem setup

Our problem formulation is a generalization of the formulation in Equation 2.1. Instead of the archetypes being a convex combination of the original data points, we optimize over a general nonlinear transformation $f(X)$ of the data under which the archetypal constraints are enforced.

The general archetypal analysis problem is the following optimization:

$$\begin{aligned} \operatorname{argmin}_{f, c_1, \dots, c_k} \quad & \sum_{i=1}^n \|f(x_i) - \sum_{j=1}^k \alpha_{ij} c_j\|^2 \\ \text{s.t.} \quad & f \text{ is approximately invertible on } X \\ & \sum_{j=1}^k \alpha_{ij} = 1, \quad i = 1, \dots, n \\ & \alpha_{ij} \geq 0, \quad i = 1, \dots, n, \quad j = 1, \dots, k \end{aligned}$$

The inclusion of f in the optimization is unique to our formulation, while previous methods either considered no transformation (i.e., $f = \text{identity}$), or considered one provided by an independent preprocessing step. Detailed discussion of such approaches is provided in Section 2. We note that our requirement that f be approximately invertible is added here to allow the mapping of archetypes $\{c_j\}_{j=1}^d$ and hypothetical (convex) combinations of them to the original feature space, for both interpretability and generative purposes, as demonstrated in Section 4.

3.2. The AAnet Autoencoder Framework

We propose a deep learning approach for solving the optimization problem in Section 3.1, by considering f as a result of a neural network we called AAnet (*Archetypal Analysis Network*). To consider the approximate invertibility constrained, we base our network on an autoencoder, where the encoder $E(x)$ yields the transformation f , and the decoder $D(x)$ yields its (approximate) inverse. Then, the convex combination constrained is ensured by our architecture choice and a novel regularization that we term the *archetypal regularization*. This regularization constrains the activations in that layer to be coefficients of the archetypal decomposition of a data point in the latent space of the neural network, and thus the archetypes themselves are naturally represented by one-hot vectors in this space.

Formally, our network is formed by an encoder $z = E(x)$ and decoder $\tilde{x} = D(z)$, with the main MSE reconstruction loss

$$\text{MSE} = \mathbb{E}_{x \in X} [\|x - \tilde{x}\|^2] = \mathbb{E}_{x \in X} [\|x - D(E(x))\|^2].$$

Then, to enforce k archetypes, we expect z to provide us with k nonlinear activations that sum up to one. However, notice than given such equality, we can in fact directly compute $\alpha_k = 1 - \sum_{j=1}^{k-1} \alpha_j$. Hence, we set the embedding layer in our network to have $k - 1$ nodes computed from the encoder layers, which we denote by $E'(x) \in \mathbb{R}^{k-1}$ and an additional virtual node yielding $z = E(x) = [E'(x), 1 - \|E'(x)\|_1]$.

The described encoder architecture choice allows us to relax the unit-equality constraint to an inequality constraint, which is more suitable for the optimization used in neural network training. Therefore, our archetypal regularization is formulated as the two constraints:

1. $\|E'(x)\|_1 \leq 1$
2. $E'(x) \geq 0$ (point-wise)

for every $x \in X$, which ensures our embedding layer provides coefficients for convex combinations of k archetypes given by the k one-hot vectors of \mathbb{R}^k . We note that the requirement of data points being well represented by these archetypes is already implicitly enforced by the MSE reconstruction loss applied after the decoding layers. The final network loss is then given by reconstruction loss + two archetypal regularizers. Thus, the encoder learns a transformation that represents the data in the bounds of a convex hull, and the decode enforces accuracy of the learned representation. See Figure 3.1 for a diagram of AAnet.

By default, AAnet can find archetypes outside the data. However, to encourage the archetypes to be tight, i.e., close to the data, we can add Gaussian noise in the latent space

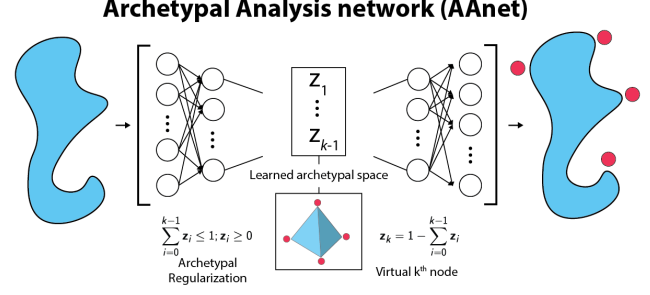


Figure 3.1. Illustrative representation of AAnet. AAnet learns a non-linear transformation of the input data (blue) such that within the embedding layer, the data fits well within a convex polytope whose vertices (red dots) represent extreme states of the data, also called archetypes. By decoding the vertices back to the input space, the archetypes can be used for exploratory data analysis.

during training. Adding noise has an effect of spreading the data out in the latent space, since the autoencoder has to reconstruct points despite the noise. This, in turn, has the effect of tightening the archetypes. This effect is shown in Figure 4.4. In essence, the hidden layer of the autoencoder is constrained to be a regular polytope of a particular dimensionality. Thus the fit is tight when the points are spread out maximally within that shape. This effect is shown in Figure 4.4. Finally, we note that the noise here is analogous to the δ parameter in Mørup & Hansen (2012), which controls the distance of the archetypes to the data.

4. Results

Here we evaluate the accuracy and performance of AAnet in finding archetypes in ground truth data with non-linearity where we know the archetypes, as well as interpretable archetypes in benchmark data from machine learning and biological datasets. We compare AAnet to seven other methods. These include three linear archetypal analysis methods: (Mørup & Hansen, 2012) (PCHA), (Chen et al., 2014), and (Javadi & Montanari, 2017), as well as k -means centroids, PCA loadings, the components found by non-negative matrix factorization (NMF), and PCHA on the latent layer of an autoencoder. We note that we excluded kernel-PCHA, which was presented in (Mørup & Hansen, 2012) as a non-linear version of PCHA. Kernel-PCHA finds archetypes in the kernel space, but is not able to then decode these into the original data space, which we require to compute the accuracy of the different methods. Instead, to still be able to compare to another non-linear archetypal analysis method, we ran PCHA on the latent layer of an autoencoder. In contrast to AAnet, the autoencoder is trained prior to, and independently of, the archetypal analysis. We used the same parameters for this autoencoder that we used for AAnet, except for removing the archetypal regularization. We also

note that PCHA on top of an autoencoder is based on the method presented in (Wynen et al., 2018), however adapted to an autoencoder (instead of a classifier) in order to be able to decode back to the data space. Full parameter details for AAnet are reported in Section A.1 and details of methods used for comparison are reported in Section A.2.

4.1. Archetypal analysis on non-linear data

To test the ability of AAnet to find archetypes in data with significant nonlinearity, we generated synthetic data with three known archetypes that we embedded into ten dimensions. Then, we applied one of two kinds of nonlinear transformations to create increasing amounts of either concavity or convexity. To generate data, we first sample an $n \times n_{at}$ matrix U whose elements are positive and i.i.d. uniformly distributed, and use it to uniformly sample a simplex via

$$S_{ij} = \frac{\log(U_{ij})}{\sum_{k=1}^{n_{at}} \log(U_{ik})}, \quad i = 1, \dots, n, \quad j = 1, \dots, n_{at},$$

where n is the number of data points and n_{at} the number of latent archetypes. The log makes the data uniform in the simplex after convex normalization. We then apply a nonlinearity to get

$$S_{nl} = S^\rho.$$

When $\rho < 1$ the data becomes convex; when $\rho > 1$ the data becomes concave. Finally, we randomly generate n_{at} archetypes in n_{dim} dimensions via a $n_{at} \times n_{dim}$ matrix A whose elements are sampled uniformly i.i.d., and project our data by

$$\text{data} = Z_{nl}A$$

into the space defined by the archetypes.

We then ran AAnet as well as the other methods on this generated data and quantified how well each method performs by computing the MSE between the ground truth archetypes with which the data was generated and the archetypes inferred by each method.

We find that with low levels of non-linearity most methods perform well and are able to find the correct archetypes (see Figure 4.1). However, when increasing the level of non-linearity all methods other than AAnet break down, with AAnet being the only method that consistently finds the right archetypes.

4.2. Scalability

Another advantage of archetypal analysis with neural networks is that it is scalable. To test this, we ran AAnet and the other methods on increasing numbers of MNIST samples (see figure 4.2 left). While PCHA runs faster on smaller data (less than 10^4 data points) AAnet has the fastest run

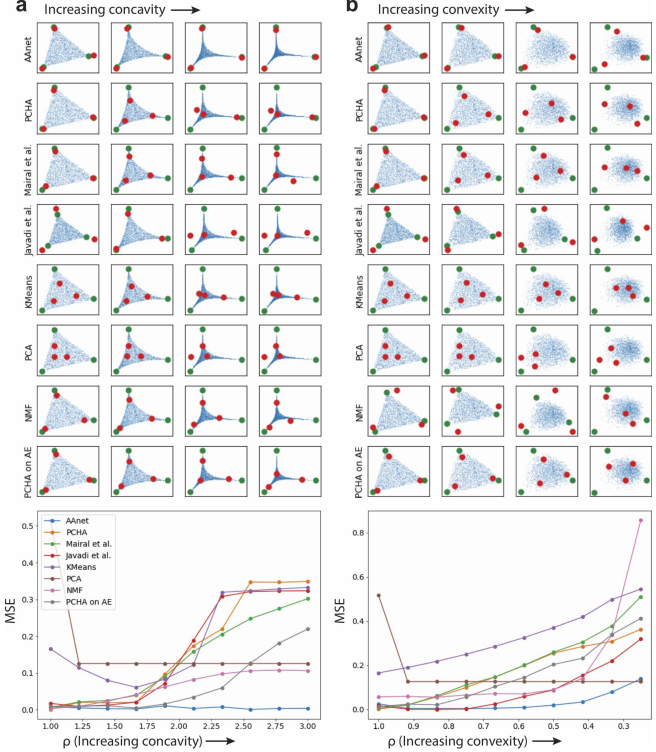


Figure 4.1. AAnet outperforms other methods on non-linear data. **(a)** Data (blue dots) is sampled from a simplex with known archetypes (green dots) and archetypes are inferred by each method (red dots). Here the non-linearity of each simplex increases with the amount of concavity of the simplex. Below, mean squared error (MSE) between ground truth archetypes and archetypes inferred by each of the 7 methods is plotted as a function of increasing concavity. **(b)** Same as (a), but with non-linearity increasing with the convexity of the simplex.

time on bigger data (more than 10^4 data points). In fact, beyond $O(10^3)$ data points the run time of AAnet is constant, while the other methods all have exponentially increasing run times with number of data points. Note, we have excluded PCHA on top of the latent layer of an autoencoder as it has run time of PCHA plus that of an autoencoder.

4.3. Optimal number of archetypes

One of the main parameters in AAnet is the number of archetypes in the model. We find that the loss function of AAnet can point us to the optimal number of archetypes, *i.e.* the true number of archetypes present in the data. Increasing the number of archetypes will cause the loss to decrease generally. However, the rate of decrease diminishes, with the loss converging at the right number of archetypes. To quantify this, we generated data with different numbers of archetypes (from 2 to 5) and ran AAnet with increasing numbers of archetypes in the model (1 to 8) and recorded the loss (see Figure 4.2b). We can observe an exponential

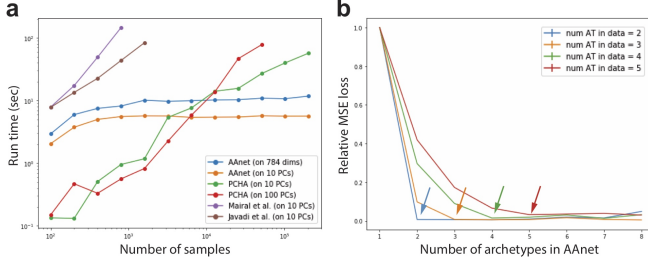


Figure 4.2. Performance of AAAnet and picking the number of archetypes. (a) Run time of AAAnet and three linear AA methods plotted as a function of the number of data points using MNIST (all digits) with and without dimensionality reduction. Only AAAnet and PCHA were able to complete on data with more than 10 principal components, and only AAAnet completed for data in the original feature space. (b) Four datasets were generated as described in Section 4.1 from simplexes with varying numbers of archetypes. MSE loss of AAAnet is reported for each dataset as a function of the number of archetypes in the model. We pick the optimal number of archetypes at the knee point (arrows).

decrease of the loss with increasing numbers of archetypes in the model. Indeed, the loss plateaus at exactly the correct number of archetypes which can be found using an elbow analysis. This is similar to the approach used by (Hart et al., 2015) in which they used an elbow analysis of the explained variance by PCHA as a function of increasing numbers of model archetypes to pick the optimal number of archetypes.

4.4. AAAnet identifies reproducible archetypes

To show that AAAnet can identify robust, reproducible archetypes, we generated archetypes for each MNIST digit 50 times using different random seeds. A subset of these images are shown in Figure 4.3a. We then calculated r^2 between archetypes identified on subsequent runs of AAAnet and random MNIST images of the same digit. For all digits, we notice a significantly higher correlation between archetypes identified in subsequent runs than between archetypes and random data points (t-test, $p < 10e - 16$). R^2 values are shown for a subset of digits in Figure 4.3b. This shows that AAAnet can robustly find the same set of archetypes across different runs.

4.5. Latent noise for tight archetypes

Archetypes can lie far outside of the data or they can be close to data points. We are able to control the tightness of the archetypes by changing the amount of Gaussian noise we add during training to the latent archetypal layer. Increasing the noise causes the convex hull to become tighter and the archetypes to come closer to the data. To illustrate this, we ran AAAnet on MNIST 4s with increasing amounts of noise (see Figure 4.4). We observe that as noise increases the archetypes move closer to and inside the data. With no

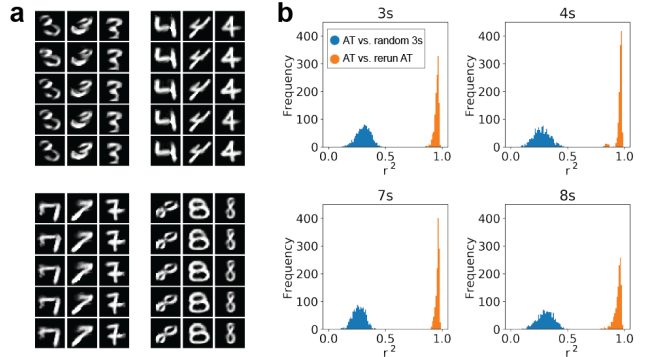


Figure 4.3. AAAnet recovers reproducible archetypes. (a) Running AAAnet repeatedly on the same dataset with different random seeds identifies similar archetypes. Archetypes were reordered to minimize distances within columns of the same digit for comparison. (b) AAAnet was run 50 times for each digit. Pearson's r^2 was calculated between all sets of archetypes and 1) all other archetypes identified for that digit (orange) and 2) random selections of images of the same digit (blue). A t-test finds $p < 10e - 16$ between the two comparisons for all digits.

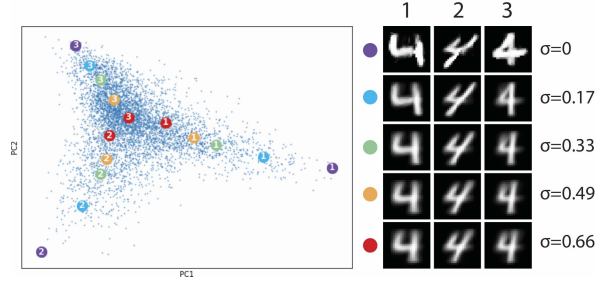


Figure 4.4. Adding increasing amounts of Gaussian noise (with standard deviation σ) to the latent archetypal layer causes the archetypes to come closer to (and inside) the data.

noise the archetypes represent hypothetical points, as they are effectively outside or in very sparse outer regions of the data. Thus, with less noise the archetypes become more extreme.

4.6. Comparison on images of MNIST digits and CelebA faces

Next, we visually investigate how AAAnet compares to the other methods on images of MNIST digits. Figure 4.5 shows all methods on MNIST 4s for three archetypes each. While most methods produce archetypes that look like different 4s, AAAnet produces the most extreme archetypes. While these still clearly resemble 4s, they give a good sense of extreme states in the data space. We note that AAAnet can produce archetypes that are outside of the data, and are thus hypothetical points. This behavior is also claimed by other methods (e.g. Javadi & Montanari (2017)). However,

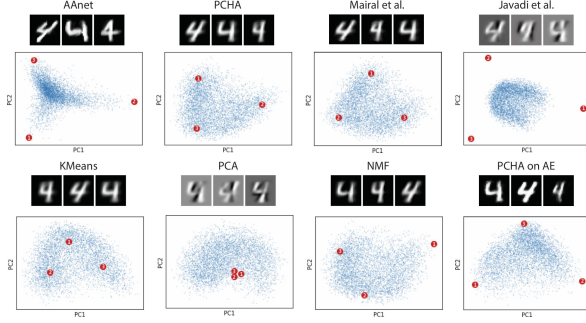


Figure 4.5. Comparison of AAAnet to other methods on MNIST 4s. Archetype images are shown for each method as well as a PCA plot of the archetypes (red) with the data projected in (blue).

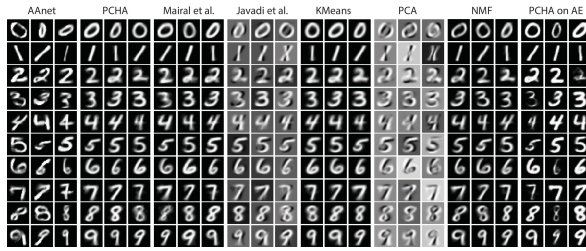


Figure 4.6. Archetypal points identified by AAAnet and other methods run on MNIST digits. The archetypes identified by AAAnet are both more diverse and more closely resemble real images than those of other methods.

with AAAnet, the resulting images are both hypothetical *and* look very much like recognizable 4s, unlike the behavior of Javadi & Montanari (2017). Figure 4.6a shows all methods on all ten MNIST digits. We performed a similar analysis on images of CelebA faces (Figure 4.7b) with ten archetypes each, showing that AAAnet produces the sharpest archetypes.

4.7. Characterization of tumor-infiltrating lymphocytes using single-cell sequencing

Tumor-infiltrating lymphocytes (TILs) are T cells, B cells and NK cells that reside in tumors. TILs are a crucial component of the immune response to cancer, yet little is known about their transcriptional repertoire (Fan & Rudensky, 2016). Although immune cell phenotypes have classically been modelled as discrete cell states, recent applications of single-cell RNA-sequencing (scRNA-seq) have found that immune cells are better described as a continuous spectrum of states (Velten et al., 2017; Azizi et al., 2018). To characterize the continuous and non-linear transcriptional state space of TILs, we applied AAAnet to a newly generated scRNA-seq dataset of 3,554 TILs selected for expression of the T cell marker CD3. We visualized the dataset using PHATE, a method we developed for visualization of high dimensional data (Moon et al., 2018). We found that 6 archetypes best describe the dataset, with each archetype



Figure 4.7. Archetypal points identified by AAAnet and other methods on CelebA faces. The archetypes identified by AAAnet are sharper and more closely resemble images of human faces than other methods.

representing a specific region of the overall state space. In Figure 4.8a, expression of T cell marker genes is plotted on a PHATE embedding after missing gene expression values were imputed using MAGIC (van Dijk et al., 2018). We also found that AAAnet was able to represent a relatively small subset of around 150 Cytotoxic T cells expressing interferon-gamma (IFN γ), but not highly expressing profilin 1 (PFN1) (See archetype 4 in Figure 4.8a).

Next, we sought to derive a gene signature of each archetype. We decoded the archetypes into the original gene expression space and calculated the percentile expression of all genes in each archetype compared to the input dataset. Figure 4.8b shows the expression of the top 10 markers for each archetype. These signatures capture known markers of T cell states, such as expression of the IFN γ receptor (IFNGR2) in archetype 1 (Naive T cells) (Curtsinger et al., 2012), high expression of perforin 1 (PRF1) in archetype 2 (Cytotoxic T cells) (Kagi et al., 1994), and upregulation of CD40L in archetype 6 (activated memory cells) (Mak & Saunders, 2006). From these results, we conclude that AAAnet is capable of characterizing the state space of a clinically-relevant biological system.

4.8. AAAnet identifies archetypal states of gut microbiomes

The microbiota residing in the human gut have an impact on human health, yet little is understood about the microbial diversity of the gut microbiome across individuals. Findings from the first datasets of gut microbial diversity suggested that the microbial profiles of individuals fit into one of several discrete clusters called enterotypes (Arumugam, 2011). However, more recent analysis suggests that gut diversity is better described by a spectrum of states enriched for different bacterial populations (Jeffery et al., 2012; Knights et al., 2014). Recently, access to cohorts of thousands of in-

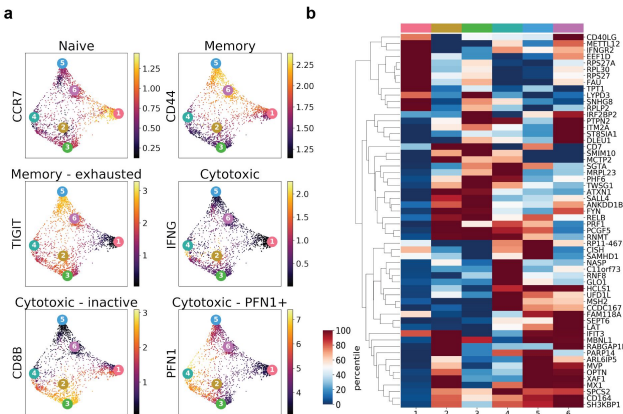


Figure 4.8. AAnet characterizes the transcriptional state space of tumor-infiltrating T cells. **(a)** PHATE visualization of 3,354 scRNA-seq profiles of mouse TILs with six archetypes projected into the embedding. Examination of markers for various T-cell states shows that each archetype corresponds to a biologically relevant cell state. **(b)** To identify gene signatures of each archetype, we projected the archetypes to the original gene expression space and ranked genes by percentile expression among all cells. Here, we show the percentile expression of the 10 genes with the highest percentile expression for each archetype.

dividual microbiome profiles make it possible to understand the space of human gut microbial composition. To show the utility of AAnet in characterizing this state space, we accessed 8,624 gut microbiome profiles from the American Gut project (Consortium, 2018). Here, bacterial diversity was determined using the 16S rRNA gene. We visualized the data using PHATE and found that the data was well described by 5 archetypes (Figure 4.9).

Examining the abundance of various bacterial populations, we find that these archetypes represent biologically relevant microbiome states. For example, two classical enterotypes are characterized by high abundance of the Bacteroides and Prevotella genera, respectively (Arumugam, 2011). We find that abundance of the Bacteroides and Prevotella genera increases in points closest to archetypes 3 and 5, respectively. This suggests that the classical enterotypes are captured by AA-net. However, we identify three other archetypes characterized by high abundance of Ruminococcaceae and Tenericutes (archetype 1), Alpha-, beta-, and Gammaproteobacteria (archetype 2), and Actinobacteria and Streptococcus (archetype 4) (Figure 4.9b). The significance of these archetypal states remains to be investigated.

Finally, we demonstrate that the archetypes capture non-linear trends in microbial abundance. To show this, we plotted the abundance of various bacterial populations within each individual as a function of the distance of that individual to a target archetype in the latent space (Figure 4.9c). Here, a LOWESS curve is fit to the data and plotted as a

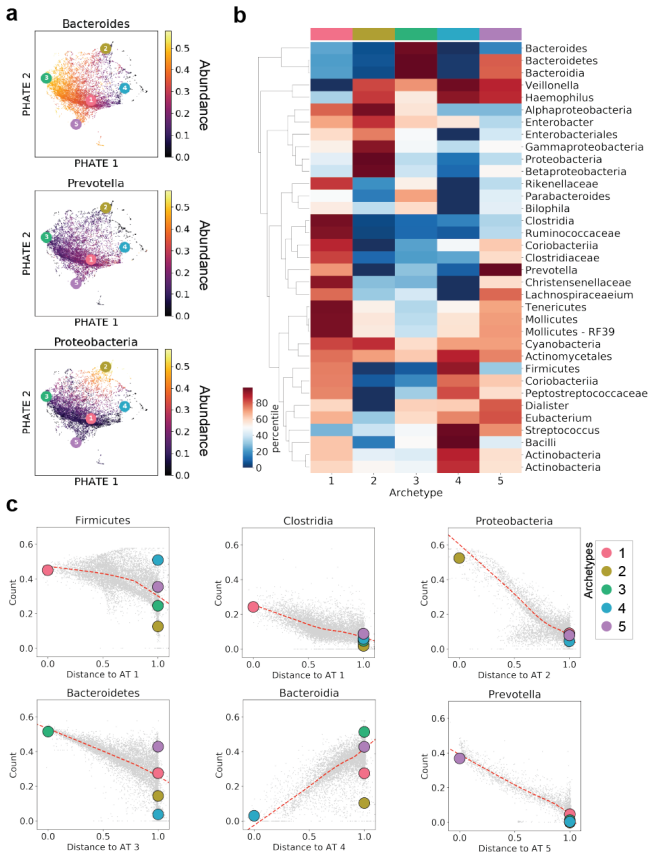


Figure 4.9. AAnet describes gut microbial diversity. **(a)** PHATE visualization of 8,624 gut microbiome profiles from the American Gut Project shows that AAnet captures archetypal states including the two classical *Bacteroides*- and *Prevotella*-enriched enterotypes. **(b)** Abundance of archetypal microbial populations expressed as a percentile compared to the original data. **(c)** AAnet captures non-linear changes in microbial abundance. Here, abundance of each population within each individual (grey dots) is plotted as a function of that individual's distance to an archetype (colored dots). LOWESS on original data is plotted (red-dashed line)

dashed red line. For example, examining abundance of the Firmicutes and Proteobacteria, we observe a clear non-linear trend in composition as individuals are increasingly distance from Archetypes 1 and 2 respectively. These results show that AAnet can be used to characterize non-linear trends across features in high dimensional biological systems.

4.9. Generating from the data geometry

Next, we describe the generative properties of AAnet. The hull learned by AAnet represents the boundary of a non-linear manifold or the geometry of the data. Combined with the ability of a neural network to decode (generate) samples from the latent space to the data space, we are able to sample from the data geometry rather than from the data density. Thus, even if the data is non-uniformly distributed,

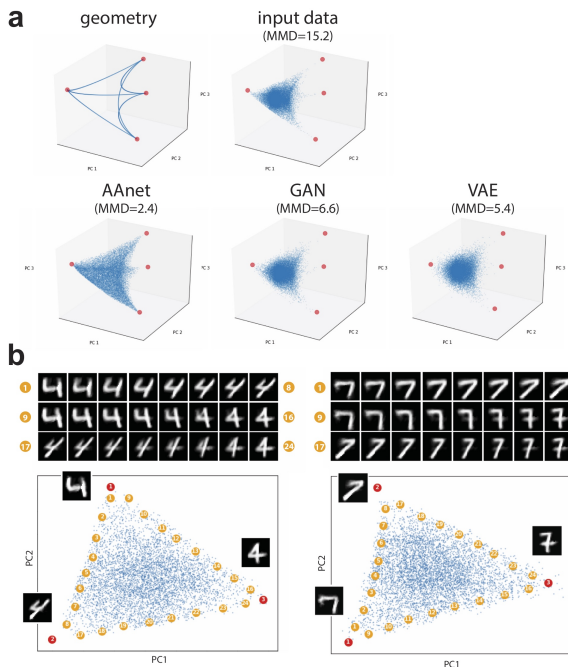


Figure 4.10. Generative properties of AAnet. **(a)** Using AAnet we can sample uniformly from the data geometry rather than from the data density. Shown is the ground truth data geometry and non-uniformly sampled input data (a, top), as well as the data generated from AAnet, a GAN, and a VAE. Only AAnet generates data throughout the geometry, instead of recreating the data density. MMD values quantify the discrepancy between each method and the ground truth geometry. **(b)** We uniformly sample trajectories between two archetypes from the AAnet. Shown are such trajectories for MNIST 4s (left) and 7s (right) between all combinations 3 archetypes. Below, PCA plots of the embedding space of the input data (blue), archetypes (red), and points on the trajectory (yellow) (b, bottom).

we can learn its geometry and then sample uniformly from this geometry and generate out to the data space.

To test this, we generated a nonlinear geometry with four archetypal points, as shown in Figure 4.10. We then sampled data non-uniformly (preferentially from the center) and trained AAnet, a GAN (Goodfellow et al., 2014), and a VAE (Kingma & Welling, 2013) on this data. GANs and VAEs are generative models and are thus able to generate samples in the data space by sampling in their latent spaces. We then sampled from the latent spaces of these three models to generate points in the data space. The GAN and VAE both generate based on the data density, while AAnet can generate from the geometry by sampling uniformly from a simplex in its latent space (see Section 4.1 for the procedure of uniformly sampling from a simplex). To quantify the ability of each model to generate from the geometry, we computed a Maximum Mean Discrepancy (MMD) (Gretton et al., 2012) (using a multiscale Gaussian kernel) between the ground truth geometry and the input data, the data gener-

ated by AAnet, the data generated by the GAN, and the data generated by the VAE. We obtained the following MMD values: 15.2, 2.4, 6.6, 5.4 for input data, AAnet, GAN, and VAE respectively, showing that AAnet has the lowest discrepancy between the generated data and the ground truth geometry.

4.10. Trajectory generation

In our final example, we demonstrate that trajectories in the AAnet latent archetypal space are meaningful. To demonstrate this, we generated samples in the data space by interpolating between pairs of archetypes in the latent space of AAnet. Figure 4.10 shows this for MNIST 4s and 7s. Walking from one archetype to another and generating data points in the input space shows that there is a gradual and meaningful change in images, *i.e.* each interpolated image looks like a meaningful convex combination of its two corresponding archetypes.

5. Conclusion

The main contribution of this paper is to change the problem formulation of archetypal analysis such that we find a transformation of the data under which the data can be described by archetypes even when the original data is not well fit by a convex polytope. For this purpose we propose a neural network that we call AAnet, which features a novel archetypal regularization that enforces a convex encoding of the data in the embedding layer. AAnet is a geometric description of the state space because it is not biased by density (Lindenbaum et al., 2018). Such descriptions are especially useful when describing biological phenotypes, because biological entities (cells, people) can exist in a non-uniform continuum of states. Using this geometric description of the data we can generate new data points by sampling uniformly from the latent archetypal geometry, which is useful for data that is sparse or missing in certain regions of the geometry. AAnet could form an important tool the area of geometry-based data generation, which has only recently been gaining prominence (Lindenbaum et al., 2018).

References

Arumugam, Manimozhiyan, e. a. Enterotypes of the human gut microbiome. *Nature*, 473(7346):174–180, May 2011. ISSN 1476-4687. doi: 10.1038/nature09944.

Azizi, E., Carr, A. J., Plitas, G., Cornish, A. E., Konopacki, C., Prabhakaran, S., Nainys, J., Wu, K., Kiseliovas, V., Setty, M., Choi, K., Fromme, R. M., Dao, P., McKenney, P. T., Wasti, R. C., Kadaveru, K., Mazutis, L., Rudensky, A. Y., and Pe’er, D. Single-Cell Map of Diverse Immune Phenotypes in the Breast Tumor Microenvironment. *Cell*,

174(5):1293–1308.e36, August 2018. ISSN 0092-8674. doi: 10.1016/j.cell.2018.05.060.

Belkin, M. and Niyogi, P. Laplacian eigenmaps and spectral techniques for embedding and clustering. In *Advances in neural information processing systems*, pp. 585–591, 2002.

Chen, Y., Mairal, J., and Harchaoui, Z. Fast and robust archetypal analysis for representation learning. In *Proceedings of the IEEE Conference on Computer Vision and Pattern Recognition*, pp. 1478–1485, 2014.

Consortium, T. A. G. American Gut: An Open Platform for Citizen Science Microbiome Research. *mSystems*, 3(3): e00031–18, June 2018. ISSN 2379-5077. doi: 10.1128/mSystems.00031-18.

Curtsinger, J. M., Agarwal, P., Lins, D. C., and Mescher, M. F. Autocrine IFN- γ promotes naive CD8 T cell differentiation and synergizes with IFN- α to stimulate strong function. *Journal of Immunology (Baltimore, Md.: 1950)*, 189(2):659–668, July 2012. ISSN 1550-6606. doi: 10.4049/jimmunol.1102727.

Cutler, A. and Breiman, L. Archetypal analysis. *Technometrics*, 36(4):338–347, 1994.

Fan, X. and Rudensky, A. Y. Hallmarks of Tissue-Resident Lymphocytes. *Cell*, 164(6):1198–1211, March 2016. ISSN 0092-8674. doi: 10.1016/j.cell.2016.02.048.

Goodfellow, I., Pouget-Abadie, J., Mirza, M., Xu, B., Warde-Farley, D., Ozair, S., Courville, A., and Bengio, Y. Generative adversarial nets. In *Advances in neural information processing systems*, pp. 2672–2680, 2014.

Gretton, A., Borgwardt, K. M., Rasch, M. J., Schölkopf, B., and Smola, A. A kernel two-sample test. *Journal of Machine Learning Research*, 13(Mar):723–773, 2012.

Hart, Y., Sheftel, H., Hausser, J., Szekely, P., Ben-Moshe, N. B., Korem, Y., Tendler, A., Mayo, A. E., and Alon, U. Inferring biological tasks using pareto analysis of high-dimensional data. *Nature methods*, 12(3):233, 2015.

Javadi, H. and Montanari, A. Non-negative matrix factorization via archetypal analysis. *arXiv preprint arXiv:1705.02994*, 2017.

Jeffery, I. B., Claesson, M. J., O'Toole, P. W., and Shanahan, F. Categorization of the gut microbiota: Enterotypes or gradients? *Nature Reviews. Microbiology*, 10(9):591–592, September 2012. ISSN 1740-1534.

Kagi, D., Vignaux, F., Ledermann, B., Burki, K., Depraetere, V., Nagata, S., Hengartner, H., and Golstein, P. Fas and perforin pathways as major mechanisms of T cell-mediated cytotoxicity. *Science*, 265(5171):528–530, 1994.

Kavanagh, K. D., Shoval, O., Winslow, B. B., Alon, U., Leary, B. P., Kan, A., and Tabin, C. J. Developmental bias in the evolution of phalanges. *Proceedings of the National Academy of Sciences*, pp. 201315213, 2013.

Kingma, D. P. and Welling, M. Auto-encoding variational bayes. *arXiv preprint arXiv:1312.6114*, 2013.

Knights, D., Ward, T. L., McKinlay, C. E., Miller, H., Gonzalez, A., McDonald, D., and Knight, R. Rethinking “Enterotypes”. *Cell host & microbe*, 16(4):433–437, October 2014. ISSN 1931-3128. doi: 10.1016/j.chom.2014.09.013.

Korem, Y., Szekely, P., Hart, Y., Sheftel, H., Hausser, J., Mayo, A., Rothenberg, M. E., Kalisky, T., and Alon, U. Geometry of the gene expression space of individual cells. *PLoS computational biology*, 11(7):e1004224, 2015.

Lindenbaum, O., Stanley, J., Wolf, G., and Krishnaswamy, S. Geometry Based Data Generation. In Bengio, S., Wallach, H., Larochelle, H., Grauman, K., Cesa-Bianchi, N., and Garnett, R. (eds.), *Advances in Neural Information Processing Systems 31*, pp. 1407–1418. Curran Associates, Inc., 2018.

Mak, T. W. and Saunders, M. E. *The Immune Response: Basic and Clinical Principles*. Elsevier Science, 2006. ISBN 978-0-12-088451-3.

Moon, K. R., van Dijk, D., Wang, Z., Gigante, S., Burkhardt, D., Chen, W., van den Elzen, A., Hirn, M. J., Coifman, R. R., Ivanova, N. B., Wolf, G., and Krishnaswamy, S. Visualizing Transitions and Structure for Biological Data Exploration. *bioRxiv*, pp. 120378, June 2018. doi: 10.1101/120378.

Mørup, M. and Hansen, L. K. Archetypal analysis for machine learning and data mining. *Neurocomputing*, 80: 54–63, 2012.

Sheftel, H., Shoval, O., Mayo, A., and Alon, U. The geometry of the pareto front in biological phenotype space. *Ecology and evolution*, 3(6):1471–1483, 2013.

Shoval, O., Sheftel, H., Shinar, G., Hart, Y., Ramote, O., Mayo, A., Dekel, E., Kavanagh, K., and Alon, U. Evolutionary trade-offs, pareto optimality, and the geometry of phenotype space. *Science*, pp. 1217405, 2012.

Szekely, P., Korem, Y., Moran, U., Mayo, A., and Alon, U. The mass-longevity triangle: Pareto optimality and the geometry of life-history trait space. *PLoS computational biology*, 11(10):e1004524, 2015.

Tendler, A., Mayo, A., and Alon, U. Evolutionary tradeoffs, pareto optimality and the morphology of ammonite shells. *BMC systems biology*, 9(1):12, 2015.

van Dijk, D., Sharma, R., Nainys, J., Yim, K., Kathail, P., Carr, A. J., Burdziak, C., Moon, K. R., Chaffer, C. L., Pattabiraman, D., Bierie, B., Mazutis, L., Wolf, G., Krishnaswamy, S., and Pe'er, D. Recovering Gene Interactions from Single-Cell Data Using Data Diffusion. *Cell*, 174(3):716–729.e27, July 2018. ISSN 0092-8674. doi: 10.1016/j.cell.2018.05.061.

Velten, L., Haas, S. F., Raffel, S., Blaszkiewicz, S., Islam, S., Hennig, B. P., Hirche, C., Lutz, C., Buss, E. C., Nowak, D., Boch, T., Hofmann, W.-K., Ho, A. D., Huber, W., Trumpp, A., Essers, M. A. G., and Steinmetz, L. M. Human haematopoietic stem cell lineage commitment is a continuous process. *Nature Cell Biology*, 19(4):271–281, April 2017. ISSN 1476-4679. doi: 10.1038/ncb3493.

Wynen, D., Schmid, C., and Mairal, J. Unsupervised learning of artistic styles with archetypal style analysis. *arXiv preprint arXiv:1805.11155*, 2018.

A. Supplement

A.1. Parameters of AAnet for various data sets

Data	Encoder	Decoder	# ATs	Last layer	Noise (σ)	Batch size	Figures
MNIST	256, 64	64, 256	3	Tanh	0.03	128	4.3, 4.4, 4.5, 4.6
CelebA	256, 256, 256	256, 256, 256	10	Tanh	0	128	4.7
Generated	256, 64	64, 256	2-5	Linear	0.03	256	4.1, 4.2, 4.10
T cell dataset	256, 128, 64	64, 128, 256	6	Linear	0.2	256	4.8
Gut microbiome	128, 64, 32	32, 64, 128	5	Linear	0.2	128	4.9

Optimizer: Adam

All layers LReLU, besides layers directly before and after archetypal layer which are linear.

Learning rate: 1e-3

Weight initialization: Xavier

A.2. Methods used for comparison

Methods used for comparison to AAnet:

Method	Source	Parameters
PCHA	(Mørup & Hansen, 2012)	default
Mairal et al.	(Chen et al., 2014)	default
Javadi et al.	(Javadi & Montanari, 2017)	default
KMeans	scikit-learn	default
PCA	scikit-learn	default
NMF	scikit-learn	default
PCHA on AE	(Mørup & Hansen, 2012)(Wynen et al., 2018)	same as AAnet